Orbital Scintigraphy with the Somatostatin Receptor Tracer ^{99m}Tc-P829 in Patients with Graves' Disease

Georg Burggasser, MD[1]; Ingrid Hurtl, MD[2]; Wolfgang Hauff, MD[1]; Julius Lukas, MD[1]; Michaela Greifeneder, MD[2]; Bamdad Heydari, MD[2]; Arnulf Thaler, MD[1]; Andreas Wedrich, MD[1]; and Irene Virgolini, MD[2,3]

[1]Department of Ophthalmology and Optometry, University of Vienna, Vienna, Austria; [2]Institute of Nuclear Medicine, Vienna City Hospital Lainz, Vienna, Austria; and [3]Ludwig Boltzmann Institute of Experimental Oncology and Photodynamic Therapy, Vienna City Hospital Lainz, Vienna, Austria

Receptors for somatostatin (SST) (SSTR) are expressed on various tumor cells as well as on activated lymphocytes. Previous data have shown that ^{99m}Tc-P829 binds with high affinity to many different types of tumor cells as well as to leukocytes via the human hSSTR2, hSSTR3, and hSSTR5 target receptors. Consequently, ^{99m}Tc-P829 was successfully introduced as a peptide tracer for tumor imaging. In this study, we evaluated the orbital uptake of ^{99m}Tc-P829 in patients with active and inactive thyroid-associated orbitopathy (TAO), accompanied by lymphocyte infiltration in the acute stage and by muscle fibrosis in the chronic stage of the disease. **Methods:** To evaluate its clinical usefulness in Graves' disease, ^{99m}Tc-P829 scintigraphy ($\approx$740 MBq) was performed in 44 patients with TAO (median duration, 19 mo; range, 1–360 mo). The clinical activity of the orbital disease was graded by the NOSPECS (*no* signs or symptoms; *o*nly signs, no symptoms; *s*igns only; *p*roptosis; *e*ye muscle involvement; *c*orneal involvement; *s*ight visual acuity reduction) classification of the American Thyroid Association, the clinical activity score (CAS), and the superonasal index (SNI). SPECT (360°) and planar studies were completed within 3 h after injection. Orbital (O) regions of interest (ROIs) were compared with temporoparietal and occipital (OCC) ROIs. Orbital uptake ratios in Graves' disease were compared with data obtained from lung cancer patients with no eye disease ($n = 22$). **Results:** Overall, ^{99m}Tc-P829 biokinetics were the same in Graves' disease patients as in lung cancer patients, showing a rapid blood clearance and visualization of the facial bones within minutes of injection. In all control patients, the orbit appeared as a "cold area," whereas visual orbital accumulation of ^{99m}Tc-P829 was found in patients with active TAO (O/OCC ratios: 1.26 ± 0.04 vs. 1.69 ± 0.04; $P < 0.01$, respectively). Patients with active eye disease ($n = 25$) presented with an increased orbital uptake of ^{99m}Tc-P829 compared with patients with inactive disease ($n = 19$; O/OCC ratio: 1.12 ± 0.05; $P < 0.01$). A statistically significant correlation was found between CAS and the orbital uptake (O/OCC ratio) values ($r = 0.90$), whereas no correlation could be documented regarding the NOSPECS classification as well as the SNI. **Conclusion:** In TAO, ^{99m}Tc-P829 yields high orbital binding with good clinical correlation. The better image quality due to the high energy of technetium, the lower radiation dose for patients and personnel, and the short acquisition protocol favor SSTR scintigraphy with ^{99m}Tc-P829 over ^{111}In-labeled compounds. The in-house availability of the radiotracer and cost-effectiveness are further advantages.

Key Words: somatostatin receptor; somatostatin receptor imaging; ^{99m}Tc-P829; ^{99m}Tc-NeoSpect; ^{99m}Tc-NeoTect; Graves' disease; thyroid associated orbitopathy

J Nucl Med 2003; 44:1547–1555

The high-level expression of peptide receptors (R) on various tumor cells compared with normal tissue or blood cells (*1,2*) provided the molecular basis for the successful use of radiolabeled somatostatin (SST) analogs as tumor tracers in nuclear medicine. Over the last decade, 5 different human hSSTR subtypes, similar in their amino acid sequences but different in their extracellular amino-terminal and intracellular carboxy-terminal domains, have been characterized in detail and have been cloned (*3–10*). These hSST subtype receptors are expressed in varying amounts by different human tumor tissues. Radiolabeled SST analogs, used for imaging purpose, have different affinities for these SSTR subtypes (*11–14*).

^{111}In-DTPA-D-Phe[1]-octreotide binds with high affinity to hSSTR2 and hSSTR5 and with moderate affinity to hSSTR3. It has been proven to be effective in diagnosing and staging SSTR-expressing tumors and their metastases (*15,16*). Despite the clinical usefulness of ^{111}In-labeled SST analogs, several attempts have been made to label hSSTR ligands with ^{99m}Tc because of its optimal decay properties and its cost-effectiveness (*17–20*). P829 (i.e., depreotide), a synthetic peptide containing a sequence that mimics the binding domain of SST, has proven to be a suitable hSSTR ligand, which can be labeled stably with [99m]Tc (*20*). Re-

cently, a broad spectrum of human tumors that can be visualized by ^{99m}Tc-P829 has been identified, including lung cancer, breast cancer, and melanoma (21). The respective target receptors for ^{99m}Tc-P829 binding are the hSSTR2, hSSTR5, and hSSTR3 subtypes (21). In the routine work-up of patients suspected of having lung cancer, the tracer has been successfully used, especially when PET technology is not available (22).

For tumor imaging, binding of the peptide–receptor complex onto the cellular surface as well as internalization have been proposed for the underlying mechanism of the SSTR tracer uptake (23). Furthermore, the expression of hSSTR subtypes by intratumoral lymphocytes, endothelial cells, or fibroblasts is an additional feature to be considered (24–28). In fact, activated T-lymphocytes have been shown to express the hSSTR2 subtype, maintaining an important role in the development of lymphocytes as well as in tumorogenesis (24). In turn, we observed that ^{99m}Tc-P829 binds to hematopoietic cells, including leukocytes (21), and is able to visualize lymphoproliferative or granulomatous disorders in vivo, as do other hSSTR radioligands (15,16).

In patients with clinically active Graves' disease, both the thyroid and the orbit present with mononuclear infiltration and inflammation evolving into fibrosis (29). T-lymphocyte infiltration of retrobulbar tissue in thyroid-associated orbitopathy (TAO) is the rationale of SSTR imaging with ^{111}In-DTPA-D-Phe[1]-octreotide. A good correlation between orbital tracer accumulation and activity of the eye disease (30,31) as graded by the NOSPECS (*n*o signs or symptoms; *o*nly signs, no symptoms; *s*igns only; *p*roptosis; *e*ye muscle involvement; *c*orneal involvement; *s*ight visual acuity reduction) classification (32), the clinical activity score (CAS) (33), the T2 relaxation time of the inferior rectus muscle in MRI (34), or ultrasonography (35) has been reported. Moreover, it was repeatedly suggested that SSTR scintigraphy could routinely be applied to select patients with TAO, who will benefit from immunosuppressive therapy (36–38) or treatment with long-acting SSTR analogs (37). However, drawbacks of ^{111}In-labeled SSTR ligand application are availability, costs, and required equipment.

In this study the orbital uptake of ^{99m}Tc-P829 was evaluated in 44 consecutive patients with active and inactive TAO. The tracer uptake was correlated to the clinical degree of TAO, and graded by NOSPECS score and CAS.

MATERIALS AND METHODS

Patients

Forty-four consecutive patients with TAO were studied. Informed consent was obtained before inclusion in the study (demographic data are included in Table 1). Twenty-five patients presented with active TAO (CAS > 2), and 19 patients presented with inactive TAO (CAS ≤ 2). Twenty-two patients, referred to our institution for staging of lung cancer, served as control subjects. Bone metastases of the head were not present in any of the lung cancer patients at the time of scintigraphy. Patients presented with TAO either at the Department of Ophthalmology of the University

of Vienna or at the Thyroid Outpatient Unit of the Vienna City Hospital Lainz. Clinical work-up was done within 1 wk of initial presentation, including assessment of thyroid disease as well as TAO in newly diagnosed patients.

Each patient underwent a clinical examination, laboratory testing of thyroid hormone function (free triiodothyronine, free L-3,5,3′,5′-tetraiodothyronine, and thyroid-stimulating hormone [TSH]), and immunologic testing including measurement of antibodies directed against the TSH receptor. Pretreatment included steroids, SST analogs, radioiodine treatment, surgery, external beam radiation, and antibody apheresis. At the time of ^{99m}Tc-P829 scintigraphy, thyroid function tests were within the normal range in 18 patients, 19 patients were hyperthyroid, 5 were latent hyperthyroid, and 2 were latent hypothyroid. For individual medication, see Table 1.

Evaluation of TAO

TAO was classified according to the NOSPECS classification of the American Thyroid Association (32) as well as by the CAS (33), based on classical signs and symptoms of inflammation. The CAS was calculated for each eye of the patient by assigning 1 point for the presence of each of the following signs: spontaneous retrobulbar pain, pain with eye movement, eyelid erythema, eyelid edema or swelling, conjunctival injection, chemosis, and swelling of the caruncle.

In addition, in all patients, the superonasal index (SNI) was evaluated using standardized echography of the orbit. To exclude a compressive optic neuropathy, standardized A-scan mode (Biovision, V-Plus) was performed in all patients for measurement of the optic nerve diameter and the extraocular muscles' diameters at 5 reference locations as defined by Ossoinig (Fig. 1) (40). The maximal time between ^{99m}Tc-P829 scintigraphy and standardized echography (SNI) was 6 wk.

Synthesis and Labeling of P829

The peptide P829 was synthesized using solid-phase peptide synthesis techniques and N-α-Fmoc chemistry, and was purified by preparative high-performance liquid chromatography as described (20,21). The instant kit containing 50 μg of the P829 peptide was used for all examinations (Nycomed-Amersham). This P829 kit was reconstituted with 1 GBq ^{99m}Tc-pertechnetate (CIS Bio International) in a final volume of 3 mL. The reconstituted product was heated for 15 min and then kept at room temperature (22°C) for 45 min. An aliquot of this preparation was used for radiochemical purity control determined by instant thin-layer chromatography (ITLC) (ITLC-SG; Gelman Sciences) developed in saturated saline (^{99m}Tc-P829 and ^{99m}Tc-microcolloid, R_f, 0–0.75) and ITLC-SG developed in pyridine:acetic acid:water (5:3:1.5) for determination of ^{99m}Tc-microcolloid (R_f, 0–0.25). For all applications, the radiochemical purity of ^{99m}Tc-P829 was >95%.

Gamma-Camera Imaging and Data Analysis

All SPECT (and planar) acquisitions were performed with an ADAC gamma camera (Vertex or Epic) equipped with a high-resolution collimator. The pulse-height analyzer window was centered on the ^{99m}Tc peak (140 keV) with a window width of ±20%. Acquisition was started at 0.5–1 h after injection and was completed within 90 min. SPECT of the skull (matrix, 64 × 64) was performed in a 360° circle in 6° steps, 40 s per step. Gamma-camera data were stored on disks. Data were processed by standard techniques using the dedicated computer software of the ADAC

TABLE 1
Demographic Data of TAO Patients Undergoing ^{99m}Tc-P829 Scintigraphy ($n = 44$)

Patient ID	DD (mo)	NOSPECS	SNI$_{od}$	SNI$_{os}$	CAS$_{od}$	CAS$_{os}$	VU$_{od}$	VU$_{os}$	Pretreatment*	OM*	TF†
006	82	4.2	5.58	5.50	0	0	−	−	1	1	1
007	53	4.2	4.92	5.39	6	6	++	++	1, 2, 4, 5, 6	6	2
008	3	2.1			5	4	++	+	1	1	2
010	103	4.2	5.23	5.46	1	1	−	−	1	1	1
012	21	4.2	6.43	5.97	4	2	+	−	1, 2, 5	1, 6	2
015	5	4.3	7.05	7.01	4	3	+	+	1, 2, 3	1	1
027	23	4.2	6.04	5.15	7	7	+++	+++	1, 2	1	2
030	26	3.1	5.00	4.88	6	7	++	++	1	1	3
018	202	4.2	5.54	6.49	2	2	+	−	3	10	4
022	1	4.2	6.82	6.04	7	7	+++	+++	1, 2	2	2
021	74	4.2	5.97	6.08	5	5	+	+	1	1	1
035	67	4.2	4.92	5.46	6	4	++	+	1, 2, 3, 5, 7	10	3
032	5	0.0	5.23	5.23	1	1	−	−	1	1	3
031	26	4.1	6.20	6.00	2	2	+	+	1, 2	1	2
037	5	4.1	5.73	5.19	6	4	++	+	1	2	3
038	22	3.2	4.84	5.08	2	2	+	+	1, 5	1	1
039	4	2.1	5.39	5.46	1	1	−	−	0	0	1
043	1	0.0			1	1	+	−	1, 8	1	2
044	4	4.1	6.01	6.16	6	5	+++	++	1	1	2
046	30	3.1	5.11	5.97	4	2	+	−	1, 2, 5	0	1
047	37	4.1	5.70	6.28	1	1	++	+	1, 2	2	1
049	10	2.0			2	2	−	−	1	1	2
050	3	1.0			0	0	−	−	1	1	1
051	25	4.2	6.24	6.47	2	3	+	++	1, 2, 5	6	1
052	54	4.3	5.86	5.35	4	6	+++	++	1, 2, 5, 11	6	1
053	4	4.1	6.01	6.43	1	1	−	−	1	1	1
054	360	4.2	6.08	5.54	7	5	+++	++	1, 4	2	1
058	17	2.0			1	1	−	−	1	2	1
062	16	4.2	6.04	5.89	6	6	+++	+++	1, 2, 9	1	1
066	48	4.2	4.26	4.38	7	7	++	++	1, 2, 3, 9	10	2
068	40	4.2	5.42	5.58	7	5	++	+	1, 2	1	2
070	10	4.1			7	5	++	+	1, 2	1	2
072	8	4.2	6.40	6.60	7	5	++	+	1	1	2
075	2	2.0			1	0	−	−	1	1	2
076f	4	2.0	5.39	5.70	2	1	−	−	1, 10	1, 10	1
079	10	4.2	5.35	5.54	7	5	+++	+++	1	1	3
081	5	2.0			2	1	+	−	1, 5, 10	10	1
077	22	4.2	5.81	5.97	1	1	+	+	1, 2, 5	10	4
064	25	4.2	5.39	5.35	3	3	+	+	1, 2, 5, 10	9, 10	2
085	4	3.0			6	4	++	++	1	1	2
086	36	4.2	5.35	5.58	1	1	−	−	1, 2, 5, 8, 11	8	1
089	10	4.1			4	5	++	++	1	1	2
072	12	4.2	6.43	6.74	6	5	+	+	2, 5, 10	2, 10	2
092	54	3.0			4	3	+	+	1	1	2

* Pretreatment and ongoing medication: 1 = carbimazole; 2 = steroids; 3 = irradiation; 4 = radioiodine; 5 = thyroid resection; 6 = apheresis; 7 = octreotide; 8 = photopheresis; 9 = β-blocking agents; 10 = thyroxin; 11 = orbital decompression according to Olivari (39).

†Thyroid function: 1 = euthyroid; 2 = hyperthyroid; 3 = latent hyperthyroid; 4 = latent hypothyroid.

ID = identification; DD = disease duration; SNI = superonasal index; od = oculus dexter (right eye); os = oculus sinister (left eye); VU = visual uptake; OM = ongoing medication; TF = thyroid function.

gamma camera with which the images had been acquired. All SPECT data were reconstructed in conventional axial, sagittal, and coronal projections using a Butterworth filter (cutoff, 0.5; order, 6). Planar acquisitions used a matrix of 256×256, 500 kilocounts were acquired. The analysis of efficacy was based on blinded evaluation of the ^{99m}Tc-P829 images. Two experienced nuclear medicine practitioners with no knowledge of the patients demo-graphic or background characteristics, medical history, clinical presentation, or results of other diagnostic tests (i.e.: SNI, CAS) independently evaluated the images for each patient.

Images were evaluated visually for the presence or absence of tracer uptake in the following areas: right orbit (RO), left orbit (LO), temporoparietal (T) skull, and occipital (OCC) skull. For semiquantitative calculation, regions of interest (ROIs) were
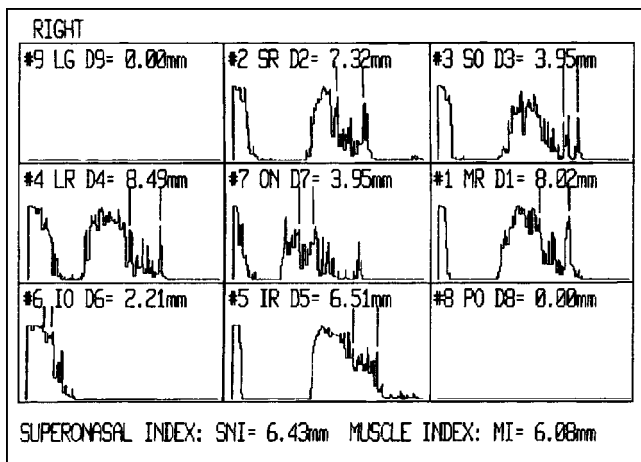
FIGURE 1. Standardized echography of extraocular muscles and optical nerve. Frames are sorted according to anatomic position. Diameters are measured by A-scan mode: #1, MR = medial rectus muscle; #2, SR = superior rectus muscle; #3, SO = superior oblique muscle; #4, LR = lateral rectus muscle; #5, IR = inferior rectus muscle; #6, IO = inferior oblique muscle; #7, ON = optic nerve. SNI is mean of diameters of 1, 2, and 3.

drawn on every skull SPECT. The mean of counts was calculated for rectangular ROIs (16 pixels) of the RO, LO, T and OCC (Fig. 2). Particular care was taken to exclude nasal or pharyngeal activity from the ROIs. Uptake ratios were calculated for RO/T and LO/T (O/T) and for RO/OCC and LO/OCC (O/OCC). All gamma-camera data were background corrected. In all lung cancer patients, SPECT studies of the chest and head as well as planar studies in anteroposterior and posteroanterior projections (chest, abdomen) were performed.

In 5 patients dynamic studies were performed with image acquisition within minutes of injection.

Analysis of skull SPECT data in lung cancer patients was performed identically to that in Graves' disease patients. Using standard nuclear medicine techniques, foci of increased labeled peptide accumulation were considered as true-positive sites of disease when corroborated by CT or MRI findings, or confirmed by histology after surgical biopsy.

Statistical Analysis

Statgraphics Plus (Statistical Graphics Corp.) for Microsoft Windows Version 4.0 and SPSS for Microsoft Windows Version 10.0 were used for statistical analysis and graphical options. Standard statistical tests performed at a confidence level of 95% included t test, simple regression analysis, ANOVA, and receiver-operating-characteristic (ROC) curve.

RESULTS

Forty-four patients with TAO were studied (37 females, 7 males; mean age, 53.8 y). Because of the wide range of the duration of the disease (median, 19 mo; range, 1–360 mo), it was not a suitable indicator for the disease activity. The mean $\pm$ SEM of the CAS was 3.5 $\pm$ 0.5 (SD, 2.31; median, 3.5) and of the NOSPECS score was 3.45 $\pm$ 0.24 (SD, 1.18; median, 4.15). The intraocular pressure was within the normal range (8–22 mm Hg) in all patients.

Overall, ^{99m}Tc-P829 biokinetics were comparable in Graves' disease patients and in lung cancer patients, showing a rapid blood clearance and visualization of the facial bones within minutes of injection. Whereas visual uptake was found in all patients with active TAO (Fig. 3), the orbit appeared as a "cold area" without ^{99m}Tc-P829 accumulation in all control patients (Fig. 4). In general, patients with active TAO ($n = 25$) showed a visually increased orbital uptake compared with that of patients with inactive disease ($n = 19$) (Table 2).
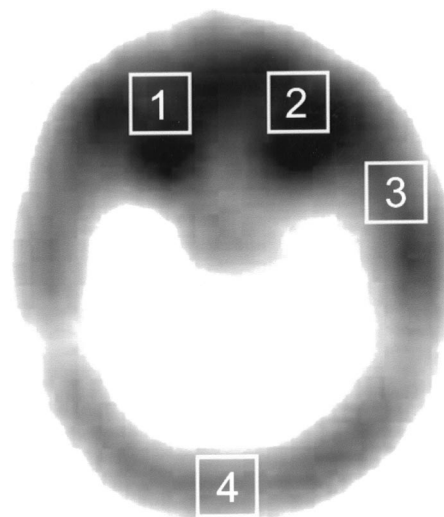
The mean of the O/OCC ratio in patients with TAO was 1.44 $\pm$ 0.03; the mean of the O/T ratio was 1.51 $\pm$ 0.03 (Table 2). No statistically significant difference of the 2 ratios ($P = 0.28$) could be proven. However, the correlation coefficient between the 2 ratios was 0.50, indicating a statistically significant, moderately strong, correlation ($R^2 = 25.36\%$; $P < 0.05$, 95% confidence level) (Table 3; Fig. 5A).

The results of orbital uptake of the ^{99m}Tc-P829 scintigraphy were in good accordance with the clinical degree of the disease, expressed by the CAS.
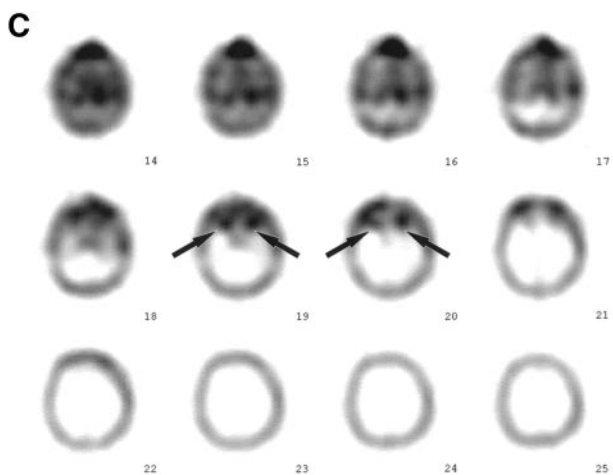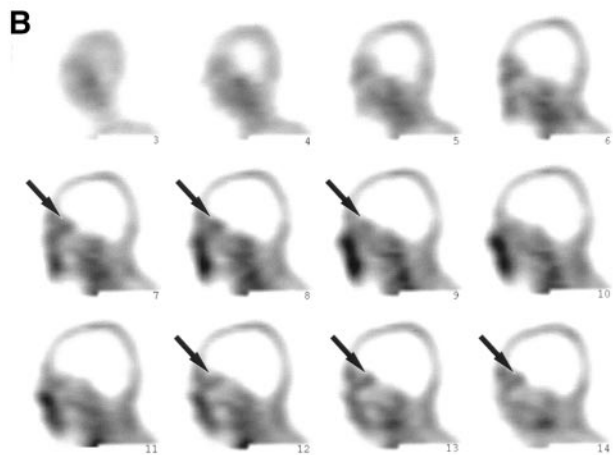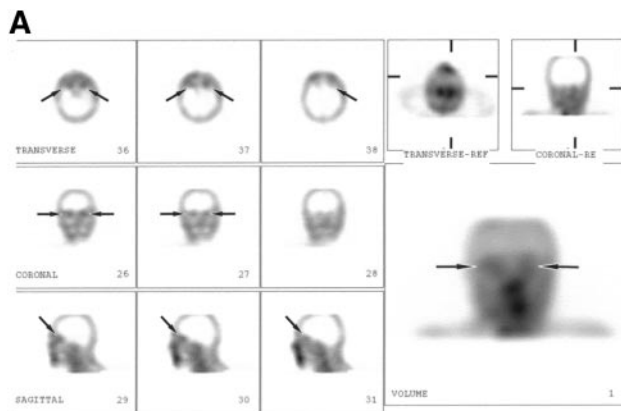
Using simple regression analysis of the O/OCC versus CAS, a statistically significant, relatively strong relationship between the variables was found ($r = 0.9$; $R^2 = 81.11\%$; $P < 0.01$, 99% confidence level) (Figs. 5B and 5C). A moderately strong relationship was observed for the O/T versus CAS ($r = 0.55$; $R^2 = 30.30\%$; $P < 0.01$, 99% confidence level) (Fig. 5D).

The ROC curve shows an area under the ROC curve of 0.970 for the O/OCC ratio (Fig. 5E). In contrast, the area under the ROC curve for the O/T ratio is only 0.707 (Fig. 5F).
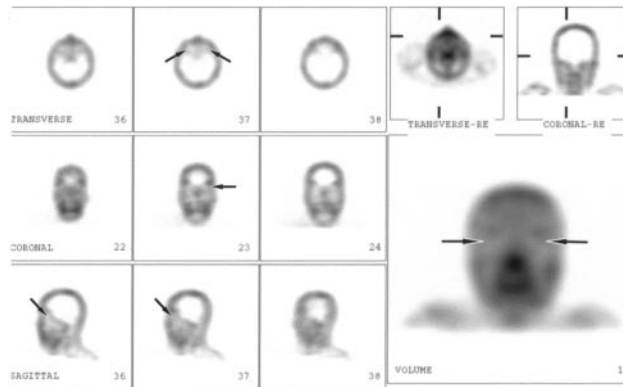
In contrast to the correlation with CAS, no correlation could be proven for the NOSPECS classification or the SNI versus all ratios calculated (Table 2).

FIGURE 2. ROIs in patient with positive ^{99m}Tc-P829 scintigraphy of orbit: 1 = right orbit; 2 = left orbit; 3 = temporoparietal reference region; 4 = occipital reference region.

FIGURE 4. [99mTc]-P829 scintigraphy (≈740 MBq) in patient of control group. Retrobulbar compartment is marked by arrow in all SPECT studies. In coronal and sagittal SPECT study, tracer accumulation in bone of lateral part of orbital roof is seen. Retrobulbar compartment is negative.

For subgroup analysis, TAO patients were grouped into patients with active TAO (CAS > 2) and patients with inactive TAO (CAS ≤ 2).

Patients with Active TAO (n = 29; CAS > 2)

The median of disease duration for this group of patients amounted to 47 mo. Only 1 patient (CAS = 7) showed a slight impairment of the visual field due to active TAO. All patients with active TAO showed visible tracer accumulation of the orbit. In general, the eye itself appeared negative, whereas the eyelid and retrobulbar tissue presented with marked accumulation of [99mTc]-P829 (Fig. 3).

The mean of the O/OCC in patients with active TAO amounted to 1.69 ± 0.04; the mean of the O/TP was 1.61 ± 0.04 (Table 2). The t test did not reveal a statistically

TABLE 2
Means with 95% LSD Intervals

Ratio	n	Mean ± SEM	SD	LL	UL
O/OCC$_{all}$	44	1.44 ± 0.03	0.37	1.40	1.48
O/T$_{all}$	44	1.51 ± 0.03	0.31	1.47	1.55
O/OCC$_{act}$	25	1.69 ± 0.04	0.29	1.63	1.75
O/T$_{act}$	25	1.61 ± 0.04	0.30	1.55	1.67
O/OCC$_{inact}$	19	1.12 ± 0.05	0.16	1.06	1.19
O/T$_{inact}$	19	1.38 ± 0.05	0.28	1.32	1.45
O/OCC$_{contr}$	22	1.26 ± 0.04	0.22	1.20	1.32
O/T$_{contr}$	22	1.18 ± 0.04	0.21	1.12	1.24

LSD = least significant differences; O/OCC$_{all}$ = orbit/occipital ratio for all patients with TAO; O/T$_{all}$ = orbit/temporoparietal ratio for all patients with TAO; O/OCC$_{act}$ = orbit/occipital ratio for all patients with active TAO; O/T$_{act}$ = orbit/temporoparietal ratio for all patients with active TAO; O/OCC$_{inact}$ = orbit/occipital ratio for all patients with inactive TAO; O/T$_{inact}$ = orbit/occipital ratio for all patients with inactive TAO; O/OCC$_{contr}$ = orbit/occipital ratio for all control patients; O/T$_{contr}$ = orbit/temporoparietal ratio for all control patients.

Means with 95% LSD intervals show mean ± SEM, SD, and lower limit (LL) and upper limit (UL) of 95% LSD intervals of various groups of tracer ratios.

FIGURE 3. (A) [99mTc]-P829 scintigraphy (≈740 MBq) in patient 022 of Table 1 with active TAO (CAS = 7 for both eyes). Retrobulbar compartment with tracer accumulation is clearly seen in all SPECT projections (arrows). (B) Sagittal SPECT study of same patient as in A: Tracer accumulation in retrobulbar compartment is clearly marked at both sides. Uptake in globes is negative; retrobulbar compartment is highly positive (arrows). In midline of head, tracer accumulation in nasal part of pharynx is seen. (C) Transverse SPECT study of same patient as in A and B: Tracer accumulation in retrobulbar compartment is clearly visible in 4 slices on both sides (arrow). Anterior to globe, slight tracer accumulation in eyelids is observed, and tracer accumulation in nasal part of pharynx, including slices beneath level of orbit, is seen.

TABLE 3
Statistical Analysis of Tracer Uptake and Correlation with CAS: Simple Regression Analysis vs. Corresponding Parameters

Ratio	O/T Correlation coefficient	O/T R^2 (%)	CAS Correlation coefficient	CAS R^2 (%)
O/OCC_{all}	0.50	25.36	0.90	81.11
O/T_{all}	—	—	0.55	30.30
O/OCC_{act}	0.42	17.87	0.75	56.99
O/T_{act}	—	—	0.66	43.85
O/OCC_{inact}	0.31	9.32	0.47	48.51
O/T_{inact}	—	—	0.25	6.26
O/OCC_{contr}	0.36	13.21	—	—

Statistical analysis of tracer uptake and correlation between corresponding ratios as well as between ratios and corresponding CAS. Abbreviations are same as those in Table 2.

significant difference between the 2 means ($P = 0.17$). The simple regression analysis yielded a moderately strong relationship between the 2 ratios (Table 3).
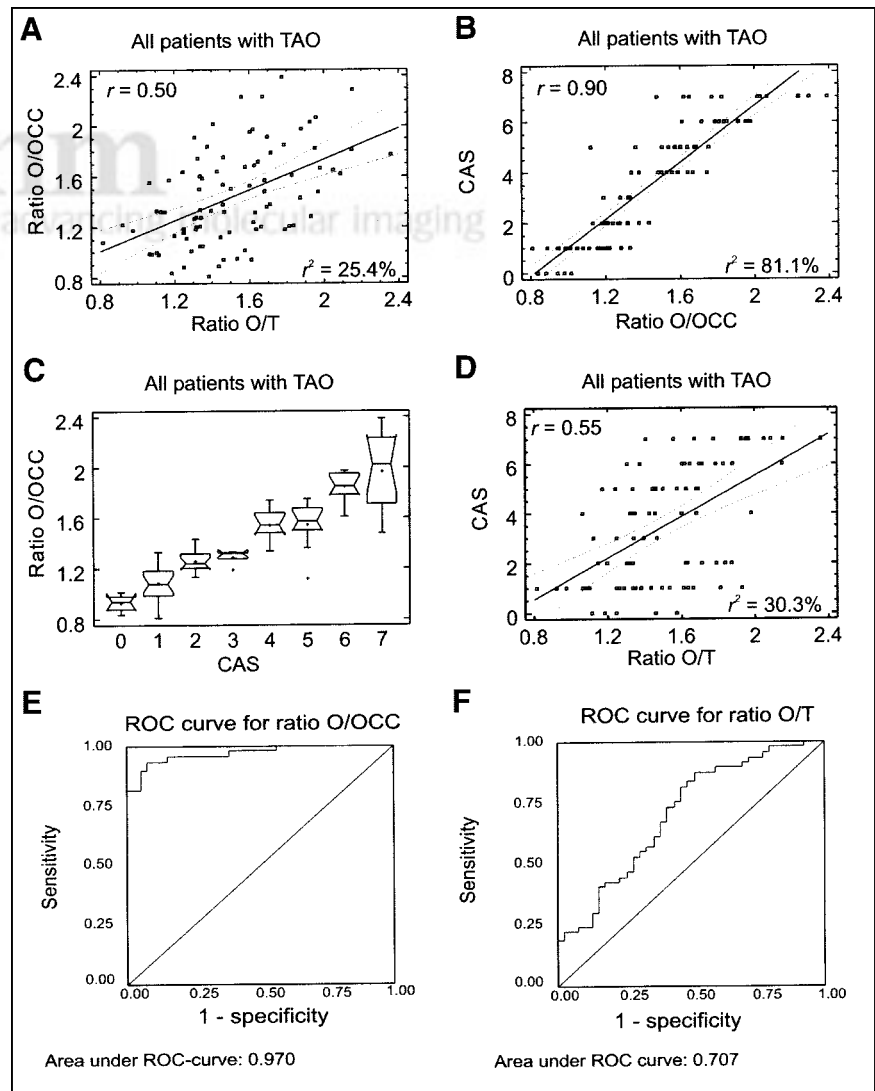
The simple regression analysis for the O/OCC versus CAS and the O/T versus CAS revealed a statistically significant, moderately strong relationship (Table 3).

In 5 patients with active TAO, dynamic studies were performed and showed ^{99m}Tc-P829 uptake in the orbits within minutes of injection.

Patients with Inactive TAO ($n = 19$; CAS ≤ 2)

Patients with only minimal clinical signs of TAO (CAS ≤ 2) were defined as patients with inactive TAO. The patients could be divided into 2 groups: patients with recently diagnosed Graves' disease of the thyroid with only minimal signs of TAO ($n = 10$) (disease duration: median, 4 mo; NOSPECS: median, 2) and patients before strabismus surgery due to muscle fibrosis ($n = 9$) with a long disease duration (median, 30 mo; NOSPECS median, 4.2).

FIGURE 5. (A) Simple regression analysis of O/T vs. O/OCC for all TAO patients demonstrates moderately strong statistically significant correlation. (B) Simple regression analysis of O/OCC vs. CAS for all TAO patients demonstrates relatively strong statistically significant correlation. (C) Box-and-whisker plot of ANOVA for O/OCC for all TAO patients demonstrates statistically significant differences between groups defined by CAS. Box part of plot extends from lower quartile to upper quartile, covering center half of sample. Center lines within each box show location of sample medians. Plus signs indicate location of sample means. Whisker extends from box to minimum and maximum values in sample, except for any outside or far outside points, which are plotted separately. (D) Simple regression analysis of O/T vs. CAS for all TAO patients demonstrates moderately strong statistically significant correlation. (E) ROC curve for O/OCC ratio. (F) ROC curve for O/T ratio.

Only slight visible tracer accumulation (visual uptake, +) was seen in 32% of patients with inactive disease (Table 1).

The mean of the O/OCC in patients with inactive TAO was 1.12 ± 0.05; the mean of the O/T was 1.38 ± 0.05 (Table 2). The t test resulted in a statistically significant difference between the 2 means ($P < 0.001$). The simple regression analysis revealed a moderately strong relationship between the 2 ratios (Table 3).

A moderately strong relationship was found in the simple regression analysis of O/OCC versus CAS; a weak relationship was found in the simple regression analysis of O/T versus CAS (Table 3).

Using multiple-sample comparison of ratios for all groups of patients with TAO, statistically significant differences at a 95% confidence level between the various groups were observed (Table 4).

To distinguish between active and inactive patients with TAO, a threshold value of 1.32 for the O/OCC ratio with a sensitivity of 0.939 and a specificity of 0.933 was determined. For the O/T ratio, the sensitivity was 0.878 with a specificity of only 0.487 at a threshold value of 1.32.

Patients with Lung Cancer (Control Group)

None of the lung cancer patients showed significant visual orbital uptake of ^{99m}Tc-P829. In some patients, tracer accumulation was seen in the orbital roof, whereas the retrobulbar space itself appeared negative (Fig. 4). This may be due to tracer accumulation in the frontal sinus or bone. The mean of the age of the control group was 63.9 y. In elderly patients, an internal frontal hyperostosis is observed commonly, which may explain the tracer accumulation in the orbital roof.

A mean of 1.26 ± 0.04 for the O/OCC and of 1.18 ± 0.04 for the T/O was calculated. Only a weak relationship between these 2 ratios could be found ($r = 0.36$; $R^2 = 13.21\%$).

A statistically significant difference between the orbital uptake of the control group and the various groups of patients with TAO is depicted in Table 4.

DISCUSSION

During the past decade, receptor-based imaging has gained widespread acceptance. Several studies have indi-

cated the clinical usefulness of the receptor-ligand binding concept for diagnostic purpose ([11–16,21]). ^{99m}Tc-P829 contains a bioactive mimetic of the presumed bioactive sequence of native SST. This amino acid sequence is the cyclic hexapeptide domain of the peptide component of ^{99m}Tc-P829, containing the pharmacophore L-tyrosine-D-tryptophan-L-lysine-L-valine, which binds to the hSSTR. Our previous studies have indicated that the hSSTR2, hSSTR3, and hSSTR5 subtypes are the target receptor subtypes ([21]). These receptors have been found in high numbers in various tumor tissues, including lung cancer, which is the primary indication for ^{99m}Tc-P829 scintigraphy ([22]). SSTR expression has also been demonstrated for lymphocytes, macrophages, and hematopoietic cells ([24,26–28]). Enhanced hSSTR expression on inflammatory cells, or an increased number of certain inflammatory cells, may provide the basis for receptor scintigraphy in autoimmune processes.

TAO is an autoimmune disease, characterized by inflammation, edema, and secondary fibrosis of the orbital tissue. The edema is due to the hydrophilic action of glycosaminoglycans secreted by activated fibroblasts. The inflammation is due to infiltration of the extraocular muscles and orbital connective tissue by lymphocytes, especially T-lymphocytes and macrophages ([30]). For the orbit, hSSTR expression has been reported for T-lymphocytes. In addition, activated fibroblasts and fibrotic muscle tissue may also express hSSTR receptor subtypes ([41]).

TAO has been extensively studied over the last decade using the SSTR ligand ^{111}In-DTPA-D-Phe^1-octreotide (OctreoScan; Mallinckrodt Medical) ([30–32,34]). Results of major studies suggest an additional prognostic parameter when applying this receptor tracer during the course of the disease. However, the routine application of ^{111}In-DTPA-D-Phe^1-octreotide is still under debate, although the scintigraphy is apt to visualize successfully the active disease in patients with TAO. The drawbacks of ^{111}In-DTPA-D-Phe^1-octreotide scintigraphy are availability of the compound, high radiation doses for patients and personnel, and acquisition time up to 48 h after injection.

To our knowledge, the clinical applicability of ^{99m}Tc-P829 scintigraphy in patients with TAO has not been re-

TABLE 4
Multiple-Sample Comparison of Various Ratios of Tracer Uptake of Different Groups of Patients

Ratio	O/OCC$_{all}$	O/OCC$_{act}$	O/OCC$_{inact}$	O/OCC$_{contr}$	Ratio	O/T$_{all}$	O/T$_{act}$	O/T$_{inact}$	O/T$_{contr}$
O/OCC$_{all}$	—	−0.251*	−0.316*	0.176*	O/T$_{all}$	—	−0.099	0.124*	0.328*
O/OCC$_{act}$	−0.251*	—	0.567*	0.427*	O/T$_{act}$	−0.099	—	0.223*	0.427*
O/OCC$_{inact}$	−0.316*	0.567*	—	−0.140*	O/T$_{inact}$	0.124*	0.223*	—	0.204*
O/OCC$_{contr}$	0.176*	0.427*	−0.140*	—	O/T$_{contr}$	0.328*	0.427*	0.204*	—

*Statistically significant difference of means.
Abbreviations are same as those in Table 2.

ported previously. Our results indicate rapid blood clearance of ^{99m}Tc-P829 after intravenous injection and accumulation in the disease-affected orbit within minutes after injection. Our study shows that the means for the orbital uptake ratios are significantly different for patients with active TAO compared with those for patients with inactive TAO. Furthermore, a statistically significant correlation between the CAS of the orbital disease and ^{99m}Tc-P829 tracer uptake in patients with TAO could be documented. The correlation of the O/OCC ratio versus CAS was better than the correlation of the O/T ratio versus CAS. A threshold value of 1.32 for the O/OCC ratio is presented with a sensitivity of 0.938 and a specificity of 0.933. Only a moderately strong, statistically significant correlation was proven for the O/OOC ratio versus O/T ratio.

The better correlation of the O/OCC ratio versus CAS may be explained by the anatomic variability of the parotid gland's size. The gland normally shows a slightly increased uptake compared with the surrounding anatomic structures, as does the nasal part of the pharynx. This can be explained by an increased hSSTR receptor expression in these glands due to an increased content of lymphatic cells, leading to a greater variability of the O/T ratio and, thus, a lower correlation with the CAS. In contrast, the O/OCC ratio reveals lower variability. The occipital bone shows a constant higher uptake at the internal occipital protuberance, because it is thicker and contains a high amount of hematopoietic cells, causing a constant high ^{99m}Tc-P829 tracer uptake. These anatomic considerations may explain the only moderately strong relationship between the O/OCC ratio and the O/T ratio.

In contrast to our study, previous studies were based on the O/T ratio (30,34). Different types of tracers were used in the clinical investigations published so far. The ROI set used in this study was similar to the ROI set described previously (32), although we chose a smaller size for each ROI. The rationale was the better image quality, which allows a clear definition of the orbits, avoiding false-positive results by excluding the uptake of the nasal part of the pharynx. However, smaller ROIs focused on the retrobulbar compartment may reveal an even better correlation than we found.

A slight higher uptake of ^{99m}Tc-P829 was observed in the control group than that in the group of patients with inactive TAO. The control group consisted predominantly of male patients; the patients with TAO were predominantly female patients. A sex-linked difference in ^{99m}Tc-P829 uptake may be the reason for the difference between these 2 groups, but a larger number of patients is needed to define a statistically significant sex-linked difference between female and male patients.

In contrast to other authors (32), no correlation between the orbital tracer uptake and the NOSPECS classification was observed in our group of patients. One reason for this observation may have been the high mean of the NOSPECS score for patients with inactive TAO. Nine patients with inactive TAO were patients presenting with fibrotic extraocular muscles and restriction of eye motility. Consequently, this resulted in a high NOSPECS score even for patients with inactive TAO.

Another explanation could be that different SST analogs vary in the hSSTR subtype binding profile: For example, in contrast to ^{99m}Tc-P829, ^{111}In-DTPA-Phe[1]-octreotide binds to hSSTR3 with moderate affinity only (21). It appears that the binding profile of ^{99m}Tc-P829 for hSSTR subtypes is highly specific for some tumor cells, as described above, and for inflammatory cells, especially for lymphocytes. On the other hand, ^{111}In-DTPA-Phe[1]-octreotide may also accumulate in fibrotic tissue in contrast to ^{99m}Tc-P829. This would explain the correlation between the NOSPECS score and orbital ratios described so far by other investigators.

Ossoinig (40) described the usefulness of the SNI measured by standardized echography in ophthalmology to define the amount of swelling of the extraocular muscles in active TAO. Two different types of active disease can be differentiated in ophthalmology: the muscle type, characterized by a high amount of swelling of the extraocular muscles; and the connective tissue type, containing a high amount of glycosaminoglycans, leading to predominant swelling of the connective tissue. Due to this fact, we could not see a direct correlation between the SNI and CAS and the orbital tracer uptake ratios. To differentiate the 2 types and for early diagnosis of compressive optic neuropathy, the SNI should be evaluated in every patient with active TAO.

The augmented image quality, as shown in Figures 3 and 4, demonstrates the high resolution allowing identification of anatomic details. In some SPECT studies, not only differentiation between the retrobulbar tissue and the eye but also specific determination of the affected extraocular muscles were possible. Whether ^{99m}Tc-P829 SPECT scintigraphy is able to differentiate the 2 different types of active TAO as described above and whether it is able to identify the affected extraocular muscles is currently unknown.

From the results of the clinical trials conducted with ^{99m}Tc-P829 in lung cancer (22), it can be concluded that the use of concomitant treatments—particularly, corticoids, calcium channel blockers, or furosemide—does not impair the diagnostic sensitivity and specificity of ^{99m}Tc-P829. A good relationship between the activity of the disease, documented as the CAS, and the tracer uptake was observed, no matter which kind of therapy was administered.

CONCLUSION

Our data show that ^{99m}Tc-P829 scintigraphy yields a high diagnostic capacity for patients with Graves' disease and TAO. Because ^{99m}Tc labeling is simple and relatively inexpensive and exhibits desirable decay characteristics, ^{99m}Tc-P829 may be a useful imaging agent in Graves' disease. The method may be applied to detect other disorders caused by inflammation, especially autoimmunologic disorders such as sarcoidosis and rheumatic diseases.

REFERENCES

1. Reubi JC, Maurer K, vonWerder K, Torhorst J, Klijn GM, Lamberts SWJ. Somatostatin receptors in human endocrine tumors. *Cancer Res.* 1987;47:551–558.

2. Virgolini I, Yang Q, Li S, et al. Cross-competition between vasoactive intestinal peptide and somatostatin for binding to tumor cell membrane receptors. *Cancer Res.* 1994;54:690–700.

3. Yamada Y, Post SR, Wang K, et al. Cloning and functional characterization of a family of human and mouse somatostatin receptors expressed in brain, gastrointestinal tract and kidney. *Proc Natl Acad Sci USA.* 1992;89:251–255.

4. Yamada Y, Reisine S, Law SF, et al. Somatostatin receptors, an expanding gene family: cloning and functional characterization of human SSTR3, a protein coupled to adenylyl cyclase. *Mol Endocrinol.* 1992;6:2136–2142.

5. Yamada Y, Kagimoto S, Kubota A, et al. Cloning, functional expression and pharmacological characterization of a fourth (hSSTR4) and fifth (hSSTR5) human somatostatin receptor subtype. *Biochem Biophys Res Commun.* 1993;195:844–852.

6. Yasuda K, Res-Domiano S, Breder CA, et al. Cloning of a novel somatostatin receptor, SST3, coupled to adenylate cyclase. *J Biol Chem.* 1992;267:20422–20428.

7. Demchyschyn LL, Srikant CB, Sunahara RK, et al. Cloning and expression of a human somatostatin-14-selective receptor variant (somatostatin receptor 4) located on chromosome 20. *Mol Pharmacol.* 1993;43:894–901.

8. Bell GI, Yasada K, Kong H. Molecular biology of somatostatin receptors. *Ciba Found Symp.* 1995;190:65–88.

9. Corness JD, Demchyschyn LL, Seeman P. A human somatostatin receptor (SSTR3), located on chromosome 22, displays preferential affinity for somatostatin-14 like peptides. *FEBS Lett.* 1993;321:279–284.

10. Rohrer L, Raulf F, Bruns C, Buetter R, Hofstaedter F, Schüle R. Cloning and characterization of a fourth human somatostatin receptor. *Proc Natl Acad Sci USA.* 1993;90:4196–4200.

11. Virgolini I, Pangerl T, Bischof C, Smith-Jones P, Peck-Radosavljevic M. Somatostatin receptor subtype expression in human tissues: a prediction for diagnosis and treatment of cancer. *Eur J Clin Invest.* 1997;27:645–647.

12. Virgolini I, Traub T, Leimer M, et al. New radiopharmaceuticals for receptor scintigraphy and radionuclide therapy. *Q J Nucl Med.* 2000;44:50–58.

13. Virgolini I, Traub T, Novotny C, et al. New trends in peptide receptor radioligands. *Q J Nucl Med.* 2001;45:153–159.

14. Virgolini I. Experience with indium and yttrium labeled somatostatin analogs. *Curr Pharm Design.* 2002;8:1781–1807.

15. Krenning EP, Kwekkeboom DJ, Bakker WH, et al. Somatostatin receptor scintigraphy with ^{111}In-DTPA-D-Phe[1] and ^{123}I-Tyr[3]-octreotide: the Rotterdam experience with more than 1000 patients. *Eur J Nucl Med.* 1993;20:716–731.

16. Virgolini I, Angelberger P, Li S, et al. *In vitro* and *in vivo* studies of three radiolabeled somatostatin analogs: ^{123}I-octreotide (OCT), ^{123}I-Tyr-[3]-OCT and ^{111}In-DTPA-D-Phe-1-OCT. *Eur J Nucl Med.* 1996;23:1388–1399.

17. Maina T, Stolz B, Albert R, Bruns C, Koch P, Maecke H. Synthesis, radiochemistry and biological evaluation of a new somatostatin analogue (SDZ 219–387) labeled with technetium-99m. *Eur J Nucl Med.* 1994;21:437–444.

18. Krois D, Riedel C, Angelberger P, Kalchberger P, Virgolini I, Lehner H. Synthesis of N-α-(6-hydrazinonicotinoyl)-octreotide: a precursor of a ^{99m}Tc-complex. *Liebigs-Annalen.* 1996;1463–1469.

19. Bangard M, Behe M, Bender H, et al. Technetium-99m-octreotide for the detection of somatostatin receptor positive (SSTR+) tumors: preliminary results [abstract]. *Eur J Nucl Med.* 1998;25:837.

20. Vallabhajosula S, Moyer BR, Lister-James J, et al. Preclinical evaluation of technetium-99m-labeled somatostatin receptor-binding peptides. *J Nucl Med.* 1996;37:1016–1022.

21. Virgolini I, Leimer M, Handmaker H, et al. Somatostatin receptor subtype specificity and in vivo binding of a novel tumor tracer, Tc[99m]-P829. *Cancer Res.* 1998;58:1850–1859.

22. Blum J, Handmaker H, Rinne N. The utility of a somatostatin type receptor binding peptide radiopharmaceutical (P829) in the evaluation of solitary pulmonary nodules. *Chest.* 1998;115:224–232.

23. Janson ET, Westlin JE, Ohrvall U, Öberg K, Lukinius A. Nuclear localization of ^{111}In after intravenous injection of ^{111}In-DTPA-D-Phe[1]-octreotide in patients with neuroendocrine tumors. *J Nucl Med.* 2000;41:1514–1518.

24. Sreedharan SP, Kodama KT, Peterson KE, Goetzl EJ. Distinct subjects of somatostatin receptors on cultured human lymphocytes. *J Biol Chem.* 1989;264:949–952.

25. Papotti M, Croce S, Bello M, et al. Expression of somatostatin receptor types 2, 3 and 5 in biopsies and surgical specimens of human lung tumors. *Virchows Arch.* 2001;439:787–797.

26. Denzler B, Reubi JC. Expression of somatostatin receptors in peritumoral veins of human tumors. *Cancer.* 1999;85:189–198.

27. Raderer M, Valencak J, Pfeffel F, et al. Somatostatin receptor expression in primary gastric versus nongastric extranodal B-cell lymphoma of mucosa-associated lymphoid tissue type. *J Natl Cancer Inst.* 1999;91:716–718.

28. Tsutsumi A, Takano H, Ichikawa K, Kobayashi S, Koike T. Expression of somatostatin receptor subtype 2 mRNA in human lymphoid cells. *Cell Immunol.* 1997;181:44–49.

29. Weetman AP. Graves' disease. *N Engl J Med.* 2000;343:1236–1248.

30. Wiersinga WM, Gerding MN, Prummel MF, Krenning EP. Octreotide scintigraphy in thyroidal and orbital Graves' disease. *Thyroid.* 1998;8:433–436.

31. Gerding MN, Van der Zant FM, Van Royen EA, et al. Octreotide-scintigraphy is a disease activity parameter in Graves' ophthalmopathy. *Clin Endocrinol.* 1999;50:373–379.

32. Gorman CA. Clever is not enough: NOSPECS is form in search of function. *Thyroid.* 1991;1:353–355.

33. Mourits MP, Koornneef L, Wiersinga WM, Prummel MF, Berghout A, vander Gaag R. Clinical criteria for the assessment of disease activity in Graves' ophthalmopathy: a novel approach. *Br J Ophthalmol.* 1989;73:639–644.

34. Kahaly G, Diaz M, Just M, Beyer J, Lieb W. Role of octreoscan and correlation with MR imaging in Graves' ophthalmopathy. *Thyroid.* 1995;5:107–111.

35. Prummel MF, Suttrop-Schulten MS, Wiersinga WM, Verbeek AM, Mourtis MP, Koornneef L. A new ultrasonographic method to detect disease activity and predict response to immunosuppressive treatment in Graves' ophthalmopathy. *Ophthalmology.* 1993;100:556–561.

36. Bartalena L, Marcocci C, Bogazzi F, et al. Relation between therapy for hyperthyroidism and the course of Graves' ophthalmopathy. *N Engl J Med.* 1998;338:73–78.

37. Leech NJ, Dayan CM. Controversies in the management of Graves' disease. *Clin Endocrinol.* 1998;49:273–280.

38. Hiromatsu Y, Kojima K, Ishisaka N, et al. Role of magnetic resonance imaging in thyroid-associated ophthalmopathy: its predictive value for therapeutic outcome of immunosuppressive therapy. *Thyroid.* 1992;2:299–305.

39. Olivari N. Thyroid-associated orbitopathy: transpalpebral decompression by removal of intraorbital fat—experience with 1362 orbits in 696 patients over 13 years. *Exp Clin Endocrinol Diab.* 1999;107:208–211.

40. Ossoinig KC. *Diagnosis and Management of Graves' Orbitopathy with Standardized Echography.* Iowa City, IA: KC Ossoinig; 2000:1–13.

41. Pasquali D, Vassallo P, Esposito D, Bonavolontà G, Bellastella A, Sinisi AA. Somatostatin receptor gene expression and inhibitory effects of octreotide on primary cultures of orbital fibroblasts from Graves' ophthalmopathy. *J Mol Endocrinol.* 2000;25:63–71.